KFUPM
Journal of Undergraduate Research International

Diamond Open Access

Article *Electrical Engineering/Physics*

Design and Modeling of a High-Efficiency Unit Concentrated Solar Thermoelectric Generator

Md. Habibur Rahman Aslam[1], Foyzul Karim[1] and Anisul Islam Suva[2*]

Cite https://doi.org/10.64589/juri/207994

Submitted: May 27, 2025 **Revised:** June 30, 2025 **Accepted:** July 07, 2025

ABSTRACT

A concentrated solar thermoelectric generator (CSTEG) is a low-maintenance, silent system that converts focused solar heat energy into electricity. However, its applications are constrained by low efficiency, high material costs, and complex thermal management. In this study, a CSTEG was designed and simulated in COMSOL to operate between 473 K and 353 K. Each leg of the CSTEG was segmented into two parts, and materials with a high dimensionless figure of merit (ZT) value were used to enhance efficiency. Compounds melt-spun with excess Te (Te-MS) ($Bi_{0.5}Sb_{1.5}Te_3$) and zone-melted $Bi_{0.4}Sb_{1.6}Te_3$ after hot deformation (HD-A-Sb1.6) were used as the p-type materials. Bi_2Te_3 -10 wt% nanocomposites and polycrystalline $Bi_2Te_{2.3}Se_{0.7}$ alloy were used as the n-type materials. The simulation yielded an open-circuit voltage of 46.2 mV, a maximum power of 28.32 mW, and a conversion efficiency of 5.69%. These results highlight the potential of material segmentation and selection in enhancing CSTEG performance for concentrated solar applications.

Keywords: solar TEG, COMSOL, thermoelectric, CSTEG

1. INTRODUCTION

Recent challenges such as global warming, climate change, and environmental degradation have driven the transition to renewable energy[1]. The sun, the source of all energy forms, enables electricity generation through photovoltaic (PV) and concentrating solar power (CSP) methods[2]. While PV converts sunlight directly into electricity, CSP converts it into heat, which can then be transformed into electricity via a thermoelectric generator (TEG) using the thermoelectric effect. Several concentrated solar thermoelectric generator (CSTEG) designs have been proposed. D. Kraemer developed a solar TEG with 4.6% efficiency operating between 473 K and 353 K[3]. L. Long et al. designed a CSTEG with 4.3% efficiency and 11.2 W maximum power at 106 × suns[4]. D. Kraemer also demonstrated 7.2% efficiency at 600 °C[5].

Optical concentrators have shown potential for improving solar thermoelectric generator (STEG) performance. Moh'd A et al. reported a 19.13% increase in power development using 20-sun concentration in a flat plate collector–TEG system[6]. Baranowski et al. modeled a STEG, achieving 15.9% efficiency under 100 suns and a hot-side temperature of 1000 °C[7].

Another effective approach involves using high-efficiency solar absorber surfaces that capture solar radiation, convert it to heat, and direct it to the TEG[8]. STEG performance can also be enhanced by electroforming carbon and copper layers on the hot side to improve thermal conductivity[9]. Kraemer et al. achieved 7.4% efficiency using spectrally selective and black paint absorbers at 211-sun concentration[10].

Despite such advances, CSTEG efficiency remains low. Improvements can be achieved by using advanced materials and optimizing geometry[11]. Segmentation further enhances performance by combining materials tailored to different temperature ranges, maximizing output across the thermal gradient[12]. Yang et al. developed and validated a segmented TEG model combining $Mg_3(Sb,Bi)_2$ and $Bi_{0.5}Sb_{1.5}Te_3$–GeTe, achieving 10.4% efficiency and 0.41 W output at $\Delta T = 440$ K[13].

In this study, a segmented CSTEG was designed based on the temperature gradient. COMSOL simulations show that it produces an open-circuit voltage of 46.2 mV and a maximum electrical power output of 28.32 mW, and a conversion efficiency of 5.69%. The use of thermally stable materials ensures uniform heat distribution and improved energy conversion.

2. SET UP SCHEMATIC AND DESIGN STRUCTURE

A hybrid solar energy conversion system combining a PV cell and thermoelectric module (Figure 1) was used to capture different parts of the solar spectrum. Parallel sunlight beams contain electromagnetic waves across various ranges, including ultraviolet (UV), visible (VIS), and infrared (IR) radiation. A concave mirror is a curved mirror that focuses parallel light rays onto a concentrated area. A selective concave mirror enhances the energy conversion by reflecting specific wavelengths. Sunlight is widely used in solar concentrators for efficient thermal and electrical conversion. A PV cell absorbs UV, VIS, and NIR light to generate electricity. An IR absorber behind the cell captures the

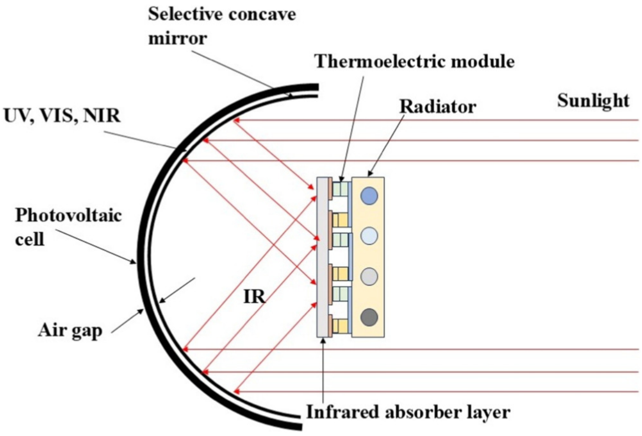

Figure 1. Schematic of hybrid solar energy converter attached with CSTEG

IR portion of sunlight channeled through a central opening or selectively transparent mirror section, heating the thermoelectric module's hot side. This module directly generates electricity from heat energy via the Seebeck effect. The radiator dissipates heat from the cold side and maintains a temperature gradient for better efficiency.

2.1. Design Structure. The designed CSTEG comprises thermoelectric materials sandwiched between hot ceramic (Al_2O_3) and cold ceramic surfaces. Ceramics exhibit excellent thermal stability, electrical insulation, and durability under temperature gradients. Heat flows from the hot-side heat source to the cold-side heat sink through thermoelectric materials. P- and n-type semiconductors are used as energy conversion materials. Two copper connectors positioned at the ends of each semiconductor leg near the cold side function as output terminals, facilitating the extraction of the direct current (DC) electrical power generated by the thermoelectric modules. Each thermoelectric leg was segmented into two parts, each of which was selected with an appropriate figure of merit (ZT) to match the operating temperature, thereby enhancing the overall conversion efficiency and performance. Figure 2 shows a schematic of the designed CSTEG module.

2.2. Boundary Conditions. The CSTEG is designed to operate within a temperature gradient, with the cold side maintained between 353 and 473 K. On the hot side, the p-type thermoelectric material functions effectively between 450 and 473 K, whereas the n-type material operates between 410 and 473 K. On the cold side, the p-type material covers 353 K to 450 K, and the n-type material operates between 353 and 410 K. These segmented temperature ranges are selected to optimize the performance and compatibility of the thermoelectric materials under realistic operating conditions. Table 1 presents the structural dimensions of the designed CSTEG unit.

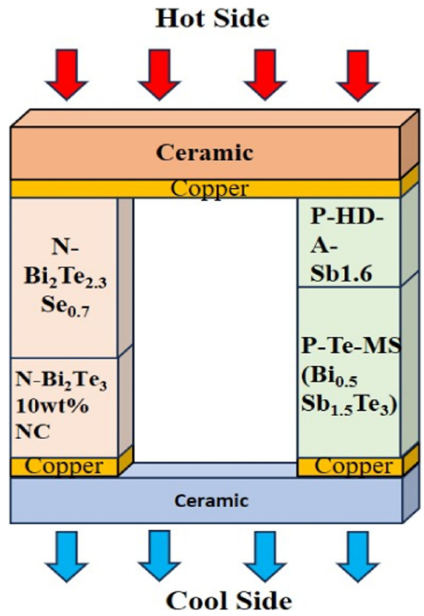

Figure 2. Schematic of designed unit CSTEG module

2.3. Materials Properties. The thermoelectric properties of materials, such as their Seebeck coefficient, electrical conductivity, and thermal conductivity, shown in Fig. 3, are critical for effective segmentation in TEGs. Selecting materials with a high ZT within a specific temperature range ensures efficient energy conversion [14]. Proper matching of these properties across segments minimizes interfacial losses and enhances overall TEG performance.

Figure 3(a) illustrates the ZT profiles of p-type $Bi_{0.5}Sb_{1.5}Te_3$ synthesized via liquid-phase compaction (Te-MS) and p-type $Bi_{0.4}Sb_{1.6}Te_3$. The ZT curves intersect at approximately 410 K, indicating a crossover in thermoelectric performance. Below this temperature, $Bi_{0.5}Sb_{1.5}Te_3$ exhibits a superior ZT, whereas above 410 K, $Bi_{0.4}Sb_{1.6}Te_3$ demonstrates enhanced performance. To

Table 1. *Geometrical measurement of designed CSTEG*

Materials	Height (mm)	Width (mm)	Depth (mm)	Operating Temperature (K)
Hot Heat exchanger (Al_2O_3)	0.5	3.9	1.4	573
Hot-side Copper	0.25	3.9	1.4	573
Hot-side p-type semiconductor ($Bi_{0.4}Sb_{1.6}Te_3$)	0.5	1.4	1.4	450–473
Cool side p-type semiconductor ($Bi_{0.5}Sb_{1.5}Te_3$)	1.0	1.4	1.4	353–450
Hot-side n-type semiconductor ($Bi_2Te_{2.3}Se_{0.7}$)	0.9	1.4	1.4	410–473
Cool side n-type semiconductor (Bi_2Te_3, 10 wt% NC)	0.6	1.4	1.4	353–410
Hot side (Terminal) Copper	0.2	1.4	1.4	353
Cool Heat exchanger (Al_2O_3)	0.3	3.9	1.4	353

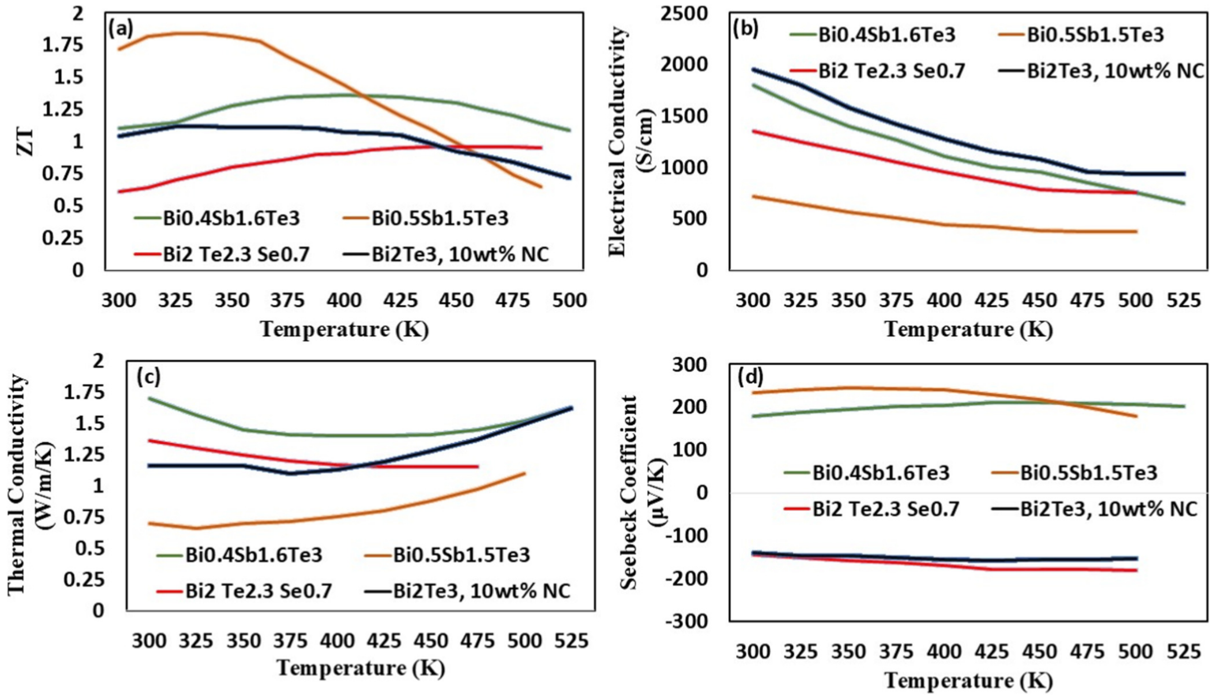

Figure 3. (a) ZT, (b) Electrical conductivity, (c) Thermal conductivity, (d) Seebeck coefficient graph against temperature for $Bi_{0.4}Te_{1.6}Te_3$ [15], $Bi_{0.5}Te_{1.5}Te_3$ [16], $Bi_2Te_{2.3}Se_{0.7}$ [17], Bi_2Te_3– wt% Nanocompound (NC) [18]

optimize the overall efficiency of the p-type leg, a segmented configuration is adopted, employing $Bi_{0.5}Sb_{1.5}Te_3$ at temperatures below 410 K and $Bi_{0.4}Sb_{1.6}Te_3$ at temperatures above this point.

Similarly, the ZT curves of n-type $Bi_2Sb_{2.3}Te_{0.7}$ and n-type Bi_2Te_3-10 wt% nanocompound (NC) intersect at approximately 445 K, signifying a transition in thermoelectric performance. Below this temperature, Bi_2Te_3-10 wt% NC delivers a higher ZT, whereas $Bi_2Sb_{2.3}Te_{0.7}$ exhibits improved performance at elevated temperatures. To enhance the overall performance of the n-type leg, a segmented design is employed, with Bi_2Te_3-10 wt% NC below 445 K and $Bi_2Sb_{2.3}Te_{0.7}$ above this temperature.

The figure also shows the Seebeck coefficient, thermal conductivity, and electrical conductivity, which are key parameters in TEG design. The Seebeck coefficient influences voltage generation, electrical conductivity affects power output, and thermal conductivity governs heat retention. Optimizing their balance is critical for achieving high conversion efficiency and overall device performance.

Ceramic (Al_2O_3) is employed as a heat exchanger in TEGs because of its excellent thermal stability, electrical insulation, and resistance to oxidation, which ensure reliable thermal transfer without short-circuiting. Copper is used as the conductor and terminal point because of its superior electrical and thermal conductivities, which enable efficient current flow and minimal energy loss. Thus, both materials are ideal for high-performance TEG applications.

3. MATHEMATICAL MODEL OF SIMULATION AND PERFORMANCE EVALUATION

The TEG was simulated in COMSOL Multiphysics 5.5 using both heat transfer and AC/DC modules to accurately model the coupled thermal and electrical behavior. The heat transfer module captures the temperature gradients and heat flow, whereas the AC/DC module simulates the electrical potential and current distribution. Their integration is essential for evaluating thermoelectric performance under realistic operating conditions.

3.1. Necessary Equations of Simulation.

Heat flows from the heat source and is absorbed by the thermoelectric materials, governed by the energy conservation equation [19]:

$$\rho C_p \cdot u \nabla T + \nabla q = Q + Q_{ted} \tag{1}$$

where ρ denotes material density (kg/m^3), C_p denotes heat capacity (J/kg · K), u indicates velocity vector (m/s), ∇T represents temperature gradient, Q is volumetric heat generation from internal sources (W/m^3), Q_{ted} denotes thermoelectric heat source or sink associated with the Thomson and Peltier effects (W/m^3), q indicates divergence of heat flux (W/m^3) and heat flux vector (W/m^2), q is $-k\nabla T$, and k denotes thermal conductivity of the material (W/m · K).

This equation describes the conductive heat transfer, including thermoelectric heat sources such as the Joule and Peltier effects.

The electric current interface models the current conservation using Ohm's law, where the magnitude of electric potential is the main variable. This enables the calculation of the electric potential, current density, and electric field of the conductive materials [19].

$$\nabla J = Q_j \tag{2}$$

where J denotes induced current density and Q_j is the current source.

$$J = \sigma E + J_e \tag{3}$$

where σ is electrical conductivity, E is the electric field, and J_e represents external current density.

$$E = -\nabla V \tag{4}$$

where V denotes electric potential.

Eqs. 5, 6, and 7 merge the electric currents and heat transfer in Solids modules [19] to capture the interrelated Peltier, Seebeck, and Thomson effects in thermoelectric devices, as described by the following equations:

$$Q = P \cdot J \tag{5}$$

where Q is volumetric heat generation from internal sources (W/m^3), P is the Peltier coefficient, and J is the induced current density.

$$P = S \cdot T \tag{6}$$

where S is the Seebeck coefficient (V/K) and T is temperature (K).

$$J_e = -\sigma S \nabla T \tag{7}$$

where J_e is external current density, σ is electrical conductivity, and ∇T is temperature difference.

These equations capture the interaction between heat and charge transport in thermoelectric materials, supporting accurate simulations of performance under nonuniform temperature distributions.

3.2. Performance Evaluation.

A TEG has an inherent internal resistance that stems from the properties of its thermoelectric legs. The internal resistance is determined using the following equation:

$$R_{int} = \sum_{i=1}^{n} \left(\frac{L}{\sigma A}\right)_i \tag{8}$$

This internal resistance leads to a voltage decrease within the device, thereby reducing the terminal voltage available at the load. The output voltage of the TEG at the load end can be expressed as

$$V = \frac{R_L}{R_L + R_{int}} \sum_{i=1}^{N} \int_{Tc}^{Th} \alpha \, dT \tag{9}$$

When an external load resistance is connected in between terminal points, the amount of current according to Ohm's law for electrical circuits is

$$I = \frac{V}{R_L + R_{int}} \tag{10}$$

This current flow generates power at the load terminals, representing the usable output power. This power can be determined using the following equation:

$$P = I^2 R_L \tag{11}$$

Electrical power is the converted form of heat energy absorbed from a heat source. The amount of absorbed heat energy is calculated using the following equation:

$$Q_h = \alpha T_h I - 0.5(I^2 R) + K(T_h - T_c) \tag{12}$$

The efficiency of this energy conversion process is expressed as a ratio of electrical power and absorbed heat.

$$\eta = \frac{P}{Q_h} \tag{13}$$

The material interface effects, contact resistances, and radiative boundary losses are generally negligible under typical operating conditions because conduction and thermoelectric effects dominate the heat and charge transport in most thermoelectric devices [20,21].

The preceding analysis clarifies the concepts involved in the energy conversion process within a TEG, which transforms heat into electricity and ultimately enables the determination of the conversion efficiency.

4. RESULTS AND DISCUSSION

The TEG performance was evaluated using the following key parameters: open-circuit voltage, load terminal voltage, load current, output power, and energy conversion efficiency. The open-circuit voltage reflects the Seebeck effect, whereas the load voltage and current indicate the response of the system to external loads. The output power indicates the energy delivery to the load, and the conversion efficiency quantifies the thermal-to-electrical energy conversion.

4.1. Thermal Distribution and Voltage Generation.

In TEG, semiconductor legs contain excess charge carriers. When a temperature gradient is applied, they absorb thermal energy from the high-temperature side and diffuse toward the cold side, converting heat into kinetic energy. In n-type materials, electrons diffuse from high- to low-temperature regions and accumulate a negative charge on the lower-temperature side. Conversely, in p-type materials, holes migrate in the same direction, leading to the build-up of positive charges on the same side. This charge separation causes a potential difference across the terminals of the TEG. The COMSOL simulation reveals that a temperature gradient of $\Delta T = 200$ K ($T_h = 473$ K and $T_c = 353$ K) generates a voltage difference of 46.2 mV, depicted in Fig. 4(b), in the TEG.

The generated voltage increases linearly with the temperature gradient, and increasing the gradient increases the voltage. Additionally, the high-temperature side, which is affected by the sun's position, seasonal changes, and weather conditions, significantly influences the voltage output. For the same material, at the high temperature of 463 K, the voltage is 42.3 mV, whereas at a 483 K temperature, the voltage increases to 50 mV. These findings describe the critical role of thermal conditions in TEG performance.

4.2. Terminal Voltage and Load Current.

When the two terminals of a TEG are connected by an external load, current flows owing to the generated potential difference. The magnitude of this current depends on the load resistance, assuming that the ohmic losses are negligible. The TEG has an internal electrical resistance that causes a voltage drop, thereby limiting the voltage available at the load terminals. For an optimal power transfer from TEG, the external load should match the internal resistance. The internal resistance is calculated using Eq. 8, the terminal

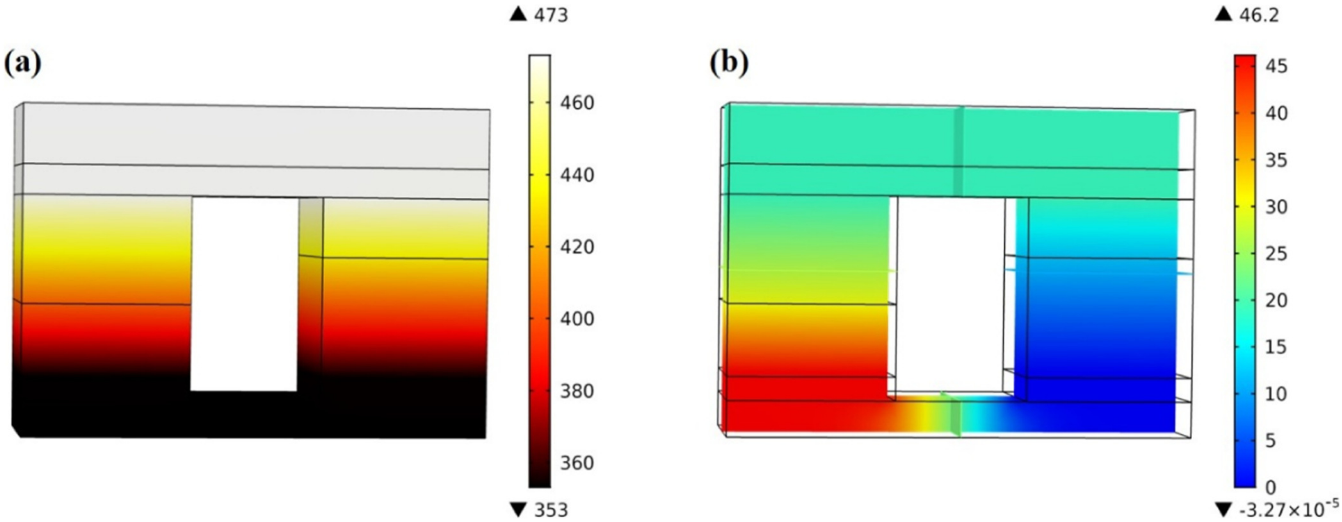

Figure 4. (a) Thermal distribution and (b) voltage distribution of the designed TEG

voltage across the load is determined using Eq. 9, and the current flowing through the load is expressed by Eq. 10.

Figure 5(a) shows the variation in the terminal voltage with the load resistance. Higher temperatures generate higher open-circuit voltages, resulting in an increased voltage across the load. Consequently, this leads to a higher load current, as demonstrated in Figure 5(b) and 5(c). These results show a direct relationship among the temperature gradient, open-circuit voltage, and current of the TEG.

A high terminal voltage and current boost the power output and efficiency in TEGs but can increase heat losses and material wear. Low voltage and current improve stability and longevity by reducing thermal stresses but result in lower power output. Balancing these factors is crucial for achieving optimal performance and durability in thermoelectric applications.

4.3. Power. Power output is a key performance metric in TEG applications because it reflects the ability of the system to convert heat energy into usable power. It is governed by the product of current and voltage across the terminal resistance. The highest amount of power transfer occurs when the external load matches the internal resistance of the TEG, ensuring optimal energy conversion. Using Eq. 8, the internal resistance of the designed device was 0.0188 Ω. The output power was subsequently evaluated using Eq. 11. Fig. 6 shows the power development of the designed TEG.

The graphs show variation in power output with load (a), terminal voltage (b), and load current (c) at three different hot-side temperatures ($T_h = 463$, 473, and 483 K). Higher hot-side temperatures (483 K) lead to higher power output across all load parameters. The maximum power output for a heat source temperature of 483 K is 33.17 mW, while for 473 K, it is 28.32 mW, and for 463 K, 23.74 mW. Throughout these measurements, the heat sink temperature is consistently maintained at 353 K. All power output curves exhibit an initial increase with increasing load resistance, reaching a peak when the value of load resistance satisfies the maximum power transfer theorem, which states that the power delivered is maximized when the external load matches the internal resistance of the source. Beyond this optimal point, as the load resistance continues to increase, the current through the circuit decreases significantly, reducing the power output. This behavior highlights the importance of load matching in the TEG design to ensure efficient energy conversion. The corresponding voltage and current values at the point of maximum power are illustrated in Fig. 6(b) and Fig. 6(c), respectively. At a hot-side temperature of 463 K, the highest power is obtained at a terminal voltage of 21.12 mV and a load current of 1.12 A. For hot-side temperatures of 473 and 483 K, the terminal voltages increase to 23.10 and 24.95 mV, with corresponding load currents of 1.22 and 1.33 A, respectively. The optimal voltage, current, and power outputs are selected based on the specific load demand.

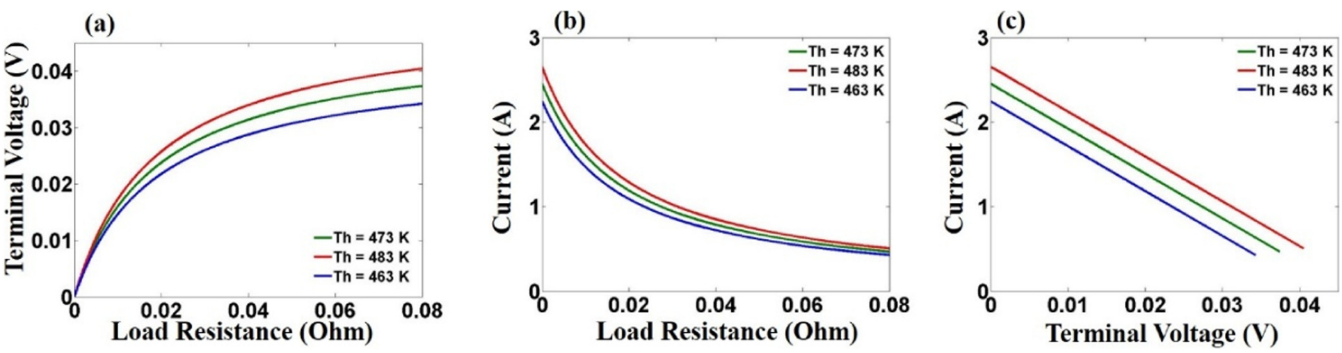

Figure 5. Graphs of (a) load terminal voltage vs. load resistance, (b) load current vs. resistance (c) load Current vs. terminal voltage

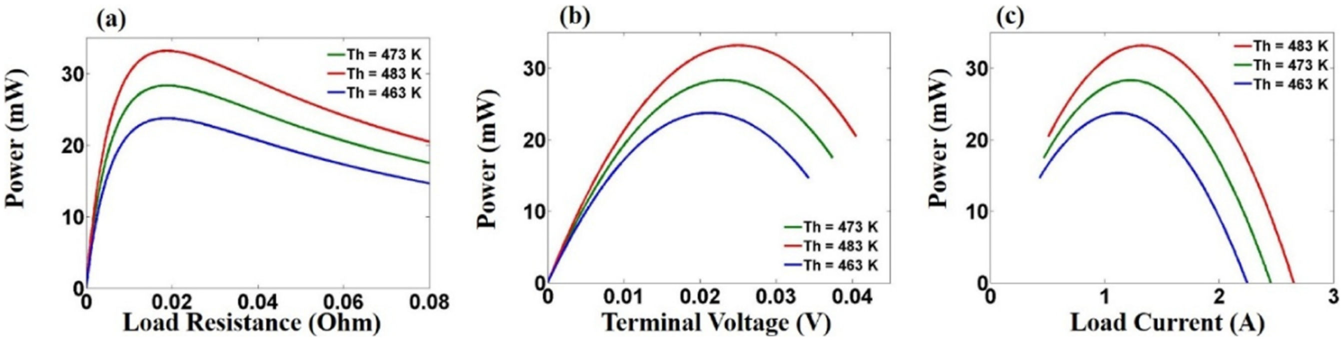

Figure 6. Graphs of (a) power vs. load resistance, (b) power vs. terminal voltage, and (c) power vs. load current

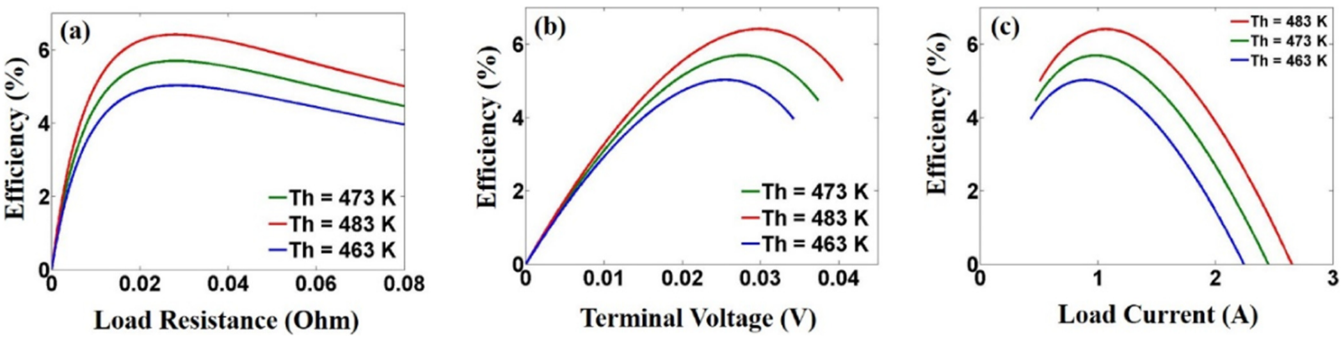

Figure 7. Graphs of (a) efficiency vs. load resistance, (b) efficiency vs. terminal voltage, and (c) efficiency vs. load current

This trend indicates that both the voltage and current at the maximum efficiency increase with increasing temperature gradients, thereby enhancing the overall performance of the TEG. An increment in hot-side temperature leads to a larger temperature gradient across the TEG, which increases the Seebeck voltage and drives more charge-carrier diffusion, resulting in greater electrical power.

4.4. Efficiency. Efficiency is crucial for TEG performance because it measures the effectiveness of heat conversion to electricity. High efficiency ensures practical viability, optimal material use, and an improved design. Figure 7 shows the efficiency trends of the designed TEG units under varying conditions. It shows how efficiency changes with resistance [Figure 7(a)], terminal voltage [Figure 7(b)], and load current [Figure 7(c)], each tested at high-temperature sides (T_h) of 463, 473, and 483 K. The outcomes show that the maximum efficiency is 6.4% (for $T_h = 483$ K), 5.69% (for $T_h = 473$ K), and 5.02% (for $T_h = 463$ K). Maximum efficiency is achieved at the same point where maximum power is obtained—that is, when the external load resistance matches the internal resistance of the TEG, which is 0.0188 Ω. The corresponding voltage and current values at the point of maximum efficiency are shown in Fig. 7(b) and Fig. 7(c). At a hot-side temperature of 463 K, the maximum efficiency is achieved at a terminal voltage of 21.12 mV and a load current of 1.12 A. As the hot-side temperature increases to 473 and 483 K, the terminal voltages increase to 23.10 and 24.95 mV, with corresponding load currents of 1.22 and 1.33 A, respectively. In each case, the heat sink temperature was 353 K.

This trend indicates that both the voltage and current at maximum efficiency increase with higher temperature gradients owing to the corresponding increase in output power. These results highlight the significant influence of the hot-side temperature on the TEG efficiency, emphasizing the critical role of operating conditions in maximizing the energy conversion performance.

Telkes employed a 50× optical concentration using a lens and achieved a 247 °C temperature gradient across thermoelectric elements composed of p- ZnSb alloy and n- Bi-based alloy, reporting a conversion efficiency of 3.35%[22]. D. Kraemer et al. reported that an efficiency of 8.6% is achievable by imposing a temperature gradient of 200 °C across an ideal thermoelectric device with $(ZT)_M = 1$ and $T_c = 20$ °C. However, they developed a solar TEG that achieved a highest efficiency of 4.6%[3]. Candadai et al. achieved 1.2% efficiency at a hot-side temperature of 280 °C for a STEG under 62-sun optical concentration, while simulations predicted 4.6% theoretical efficiency at a temperature gradient of 270 °C[23]. Pereira et al. investigated a solar TEG with $Si_{80}Ge_{20}$ and a TiAlN/SiO_2 PV absorber, achieving a maximum efficiency of 1.8%[24]. The analysis was limited to the thermal model of the solar TEG, excluding thermoelectric effects, owing to the significantly low energy conversion efficiency (approximately 3%) of Bi_2Te_3-based commercial thermoelectric modules[25,26]. However, our model obtains a peak efficiency of 5.69% at a 120 °C temperature difference ($T_h = 473$ K, $T_c = 353$ K), demonstrating improved performance over conventional modules.

5. CONCLUSIONS

A new model of a solar TEG unit was designed and simulated to enhance the efficiency via segmentation. The proposed approach optimizes the temperature gradient across a thermoelectric converter to achieve higher output energy parameters. Each leg of the

CSTEG was segmented into two parts, and materials with high ZT values were used to enhance the efficiency. The melt-spun with excess Te (Te-MS) compound ($Bi_{0.5}Sb_{1.5}Te_3$) and zone-melted $Bi_{0.4}Sb_{1.6}Te_3$ after hot deformation (HD-A-Sb1.6) were used as the p-type materials. Bi_2Te_3 -10 wt% nanocomposites and polycrystalline $Bi_2Te_{2.3}Se_{0.7}$ alloy were used as the n-type materials.

The newly designed COMSOL-simulated concentrated solar TEG model demonstrated a promising electrical performance at low temperature gradients. The model developed an open circuit voltage of 46.2 mV at 120 K ($T_h = 573$ K, $T_c = 453$ K), achieving a maximum power output of 28.32 mW and an efficiency of 5.69%. The effects of increasing and decreasing temperature gradients were also investigated, and a 10 K increment was observed to increase the voltage to 49.9 mV and power to 33.17 mW. Conversely, a 10 K decrease significantly decreased voltage to 42.25 mV and power to 23.74 mW, resulting in an efficiency of 5.02%.

The simulation results demonstrate that thermoelectric energy conversion performance can be significantly enhanced through strategic segmentation and appropriate material selection. Thus, segmented CSTEGs are promising candidates for efficient solar thermal energy harvesting, particularly for low-temperature-range applications.

This study is limited to idealized simulations, excluding real-world factors like contact resistance, material degradation, and environmental variations. Future work should include experimental validation, practical integration, and advanced segmentation/material strategies to improve efficiency.

AFFILIATIONS AND AUTHOR DETAILS

Undergraduate Author

Md. Habibur Rahman Aslam – *Electrical & Electronic Engineering, Chittagong University of Engineering and Technology, Bangladesh;* 0009-0008-0751-9645
Email: 06habib05@gmail.com

Author

Foyzul Karim – *Electrical & Electronic Engineering, Chittagong University of Engineering and Technology, Bangladesh;* 0009-0007-8318-0519
Email: u1902169@student.cuet.ac.bd

Corresponding Author

Anisul Islam Suva – *Research Mentor, Institute of Energy Technology, Chittagong University of Engineering and Technology, Bangladesh;* 0009-0000-7967-7548
Email: anisulislam.me@cuet.ac.bd

ACKNOWLEDGEMENTS

The authors acknowledge the support and resources provided by the COMSOL Community. The extensive user forums, tutorials, and shared simulation insights greatly facilitated the modeling and validation process in this study. The collaborative knowledge base offered by COMSOL users worldwide significantly contributed to overcoming technical challenges and improving simulation accuracy.

CONFLICTS OF INTEREST

The authors declare that there are no conflicts of interest regarding the publication of this manuscript.

FINANCIAL DISCLOSURE

The authors received no specific funding for this work.

REFERENCES

(1) Adrian, Maisarah, et al. "Energy transition towards renewable energy in Indonesia." *Heritage and Sustainable Development* 5.1 (2023): 107–118.

(2) Desideri, Umberto, and Pietro Elia Campana. "Analysis and comparison between a concentrating solar and a photovoltaic power plant." *Applied energy* 113 (2014): 422–433.

(3) Kraemer, Daniel, et al. "High-performance flat-panel solar thermoelectric generators with high thermal concentration." *Nature materials* 10.7 (2011): 532–538.

(4) Li, Long, et al. "Combined solar concentration and carbon nanotube absorber for high performance solar thermoelectric generators." *Energy Conversion and Management* 183 (2019): 109–115. Fan, Shufen, et al. "Influence of nanoinclusions on thermoelectric properties of n-type Bi_2 Te_3 nanocomposites." *Journal of Electronic materials* 40 (2011): 1018–1023.

(5) Kraemer, Daniel, et al. "Concentrating solar thermoelectric generators with a peak efficiency of 7.4%." *Nature Energy* 1.11 (2016): 1–8.

(6) Al-Nimr, M. A., B. M. Tashtoush, M. A. Khasawneh, and I. Al-Keyyam. "A Hybrid Concentrated Solar Thermal Collector/Thermo-Electric Generation System." *Energy*, vol. 134, 2017, pp. 1001–1012. *Elsevier*, https://doi.org/10.1016/J.ENERGY.2017.06.093.

(7) Baranowski, L. L., G. J. Snyder, and E. S. Toberer. "Concentrated Solar Thermoelectric Generators." *Energy & Environmental Science*, vol. 5, no. 9, 2012, pp. 9055–9067. *Royal Society of Chemistry*, https://doi.org/10.1039/C2EE22248E

(8) Kraemer, D., B. Poudel, H. P. Feng, J. C. Caylor, B. Yu, X. Yan, Y. Ma, et al. "High-Performance Flat-Panel Solar Thermoelectric Generators with High Thermal Concentration." *Nature Materials*, vol. 10, 2011, pp. 532–538. *Nature Publishing Group*, https://doi.org/10.1038/nmat3013.

(9) Piarah, W. H., Z. Djafar, A. S. Rosali, A. Halim, and B. H. J. Mustofa. "The Effect of Copper Coating on the Hot-Side on the Performance of a Thermoelectric Generator Using the Electroforming Method." *International Journal of Design & Nature and Ecodynamics*, vol. 17, no. 6, 2022, pp. 823–830. https://doi.org/10.18280/IJDNE.170602.

(10) Kraemer, D., Q. Jie, K. McEnaney, F. Cao, W. Liu, L. A. Weinstein, J. Loomis, Z. Ren, and G. Chen. "Concentrating Solar Thermoelectric Generators with a Peak Efficiency of 7.4%." *Nature Energy*, vol. 1, 2016, pp. 1–8. *Nature Publishing Group*, https://doi.org/10.1038/nenergy.2016.153.

(11) Chen, Wei-Hsin, and Yi-Bin Chiou. "Geometry design for maximizing output power of segmented skutterudite thermoelectric generator by evolutionary computation." *Applied Energy* 274 (2020): 115296.

(12) Snyder, G. J., and T. S. Ursell. "Thermoelectric Efficiency and Compatibility." *Physical Review Letters*, vol. 91, no. 14, 2003, p. 148301. https://doi.org/10.1103/PhysRevLett.91.148301.

(13) Yang, Kai-Yu, et al. "General Screening Rules and Segmented Optimization Strategy for Efficient Thermoelectric Devices Validated by $Mg_3(Sb,Bi)_2$ and $Bi_{0.5}Sb_{1.5}Te_3$-GeTe Module." *Advanced Science*, first published 5 May 2025, https://doi.org/10.1002/advs.202502832.

(14) Chen, Wei-Hsin, et al. "Optimization of a segmented thermoelectric generator with various doping amounts using central composite design, multi-objective genetic algorithm, and artificial neural network." *Energy* 316 (2025): 134469.

(15) Xu, Z. J., et al. "Enhanced thermoelectric and mechanical properties of zone melted p-type (Bi, Sb) 2Te3 thermoelectric materials by hot deformation." *Acta Materialia* 84 (2015): 385–392.

(16) Kim, Sang Il, et al. "Dense dislocation arrays embedded in grain boundaries for high-performance bulk thermoelectrics." *Science* 348.6230 (2015): 109–114.

(17) Hu, Lipeng, et al. "Point defect engineering of high-performance bismuth-telluride-based thermoelectric materials." *Advanced Functional Materials* 24.33 (2014): 5211–5218.

(18) Fan, Shufen, et al. "Influence of nanoinclusions on thermoelectric properties of n-type Bi2Te3 nanocomposites." *Journal of Electronic materials* 40 (2011): 1018–1023.

(19) Prasad, Asutosh, and Raj CN Thiagarajan. "Multiphysics modeling and multilevel optimization of thermoelectric generator for waste heat recovery." *Proceedings of the COMSOL Conference*. 2018.

(20) Zebarjadi, M., et al. "Perspectives on Thermoelectrics: From Fundamentals to Device Applications." *Energy & Environmental Science*, vol. 5, no. 1, 2012, pp. 5147–5162. https://doi.org/10.1039/C1EE02497C.

(21) Baranowski, L. L., G. J. Snyder, and E. S. Toberer. "Concentrated Solar Thermoelectric Generators." *Energy & Environmental Science*, vol. 5, no. 7, 2012, pp. 9055–9067. https://doi.org/10.1039/C2EE22248E.

(22) Telkes, M. "Solar Thermoelectric Generators." *Journal of Applied Physics*, vol. 25, 1954, pp. 765–777.

(23) Candadai, A. A., V. P. Kumar, and H. C. Barshilia. "Performance Evaluation of a Natural Convective-Cooled Concentration Solar Thermoelectric Generator Coupled with a Spectrally Selective High Temperature Absorber Coating." *Solar Energy Materials and Solar Cells*, vol. 145, 2016, pp. 333–341. https://doi.org/10.1016/J.SOLMAT.2015.10.040.

(24) Pereira, A., et al. "High Temperature Solar Thermoelectric Generator–Indoor Characterization Method and Modeling." *Energy*, vol. 84, 2015, pp. 485–492. https://doi.org/10.1016/J.ENERGY.2015.03.053.

(25) Jaziri, N., A. Boughamoura, J. Müller, B. Mezghani, F. Tounsi, and M. Ismail. "A Comprehensive Review of Thermoelectric Generators: Technologies and Common Applications." *Energy Reports*, vol. 6, 2020, pp. 264–287. https://doi.org/10.1016/j.egyr.2019.12.011.

(26) Maksymuk, M., B. Dzundza, O. Matkivsky, I. Horichok, R. Shneck, and Z. Dashevsky. "Development of the High Performance Thermoelectric Unicouple Based on Bi_2Te_3 Compounds." *Journal of Power Sources*, vol. 530, 2022, Article 231301. https://doi.org/10.1016/j.jpowsour.2022.231301.